Rates of Electronic Energy Transfer in Conformationally Flexible Bichromophoric Macrocyclic Complexes: A Combined Experimental and Molecular Modeling Study

Evan G. Moore,[†] Paul V. Bernhardt,[†] Anatolio Pigliucci,[‡] Mark J. Riley,*[,†] and Eric Vauthey[‡]

Department of Chemistry, School of Molecular and Microbial Science, University of Queensland, Brisbane, 4072, Australia, and Department of Physical Chemistry, University of Geneva, 30 quai Ernest Ansermet CH-1211 Geneva, Switzerland.

Received: June 23, 2003

Electronic energy transfer (EET) rate constants between a naphthalene donor and anthracene acceptor in $[ZnL^{4a}](ClO_4)_2$ and $[ZnL^{4b}](ClO_4)_2$ were determined by time-resolved fluorescence where L^{4a} and L^{4b} are the trans and cis isomers of 6-((anthracen-9-yl-methyl)amino)-6,13-dimethyl-13-((naphthalen-1-yl-methyl)amino)-1,4,8,11-tetraazacyclotetradecane, respectively. These isomers differ in the relative disposition of the appended chromophores with respect to the macrocyclic plane. The trans isomer has an energy transfer rate constant (k_{EET}) of 8.7×10^8 s^{-1}, whereas that of the cis isomer is significantly faster (2.3×10^9 s^{-1}). Molecular modeling was used to determine the likely distribution of conformations in CH_3CN solution for these complexes in an attempt to identify any distance or orientation dependency that may account for the differing rate constants observed. The calculated conformational distributions together with analysis by ^1H NMR for the $[ZnL^{4a}]^{2+}$ trans complex in the common *trans*-III N-based isomer gave a calculated Förster rate constant close to that observed experimentally. For the $[ZnL^{4b}]^{2+}$ cis complex, the experimentally determined rate constant may be attributed to a combination of *trans*-III and *trans*-I N-based isomeric forms of the complex in solution.

Introduction

With applications in a variety of areas such as light harvesting,[1,2] artificial photosynthesis,[3,4] energy transfer dye laser operation,[5] photochemical synthesis,[6] polymer photophysics,[7] and molecular devices such as polymeric light emitting diodes,[8] the deactivation of an electronically excited chromophore by electronic excitation (or energy) transfer (EET) and the mechanism by which this deactivation is achieved continues to receive significant attention.

The expression for an intramolecular EET process in a bichromophoric system is most often represented by

$$D^* - L - A \xrightarrow{k_{EET}} D - L - A^*$$

The initial electronic excitation energy localized on the donor, D*, is transferred to an acceptor, A, with concomitant quenching of the donor and sensitization of acceptor fluorescence. In this case, L denotes an inert linker which may play the dual role of connecting the two chromophores and possibly facilitating the EET process.

The overall rate constant of energy transfer, k_{EET}, can be attributed to both Coulombic (approximated by dipole−dipole) and exchange contributions (eq 1)

$$k_{EET} = k_{EET}^{dd} + k_{EET}^{ex} \tag{1}$$

Förster[9] and Dexter[10] have developed expressions for Coulombic and exchange interactions, respectively. For dipole−dipole induced EET, the Förster expression in terms of measurable spectroscopic quantities is given by eq 2[9]

$$k_{EET}^{dd} = \frac{9000 \ln(10) \kappa^2 \Phi_D J_{dd}}{128 \pi^5 n^4 N_A \tau_D R^6} \tag{2}$$

where κ^2 is an orientation factor, Φ_D is the fluorescence quantum yield of the donor, n is the refractive index of the medium, N_A is Avogadro's number, τ_D is the fluorescence lifetime of the donor in the absence of the acceptor, and R is the donor−acceptor separation. J_{dd} is the spectral overlap integral defined by eq 3

$$J_{dd} = \int_0^\infty \frac{\bar{F}_D(\bar{\nu}) \bar{\epsilon}_A(\bar{\nu})}{\bar{\nu}^4} \, d\bar{\nu} \tag{3}$$

where $\bar{F}_D$ is the donor fluorescence spectrum normalized to unit area, $\bar{\epsilon}_A$ is the acceptor's absorption spectrum expressed by its molar extinction coefficient (M^{-1} cm^{-1}), and $\bar{\nu}$ is the wavenumber (cm^{-1}).

The corresponding expression for the exchange interaction EET rate constant derived by Dexter is given in eq 4[10]

$$k_{EET}^{ex} = \frac{2\pi}{\hbar} K J_{ex} \exp(-2R/L) \tag{4}$$

where L is an average van der Waals radius for the initial and final molecular orbitals of the donor−acceptor system, R is the donor−acceptor separation, K is a numerical constant which, unlike the Förster formulation, cannot be determined from measurable spectroscopic data, and J_{ex} is the exchange interaction integral of spectral overlap

$$J_{ex} = \int_0^\infty \bar{F}_D(\bar{\nu}) \bar{\epsilon}_A(\bar{\nu}) \, d\bar{\nu} \tag{5}$$

* To whom correspondence should be addressed. E-mail: m.riley@uq.edu.au.
[†] University of Queensland.
[‡] University of Geneva.

10.1021/jp035781f CCC: $25.00
Published on Web 09/23/2003

CHART 1: Photoactive Bichromophores and Model Compounds Described in This Study

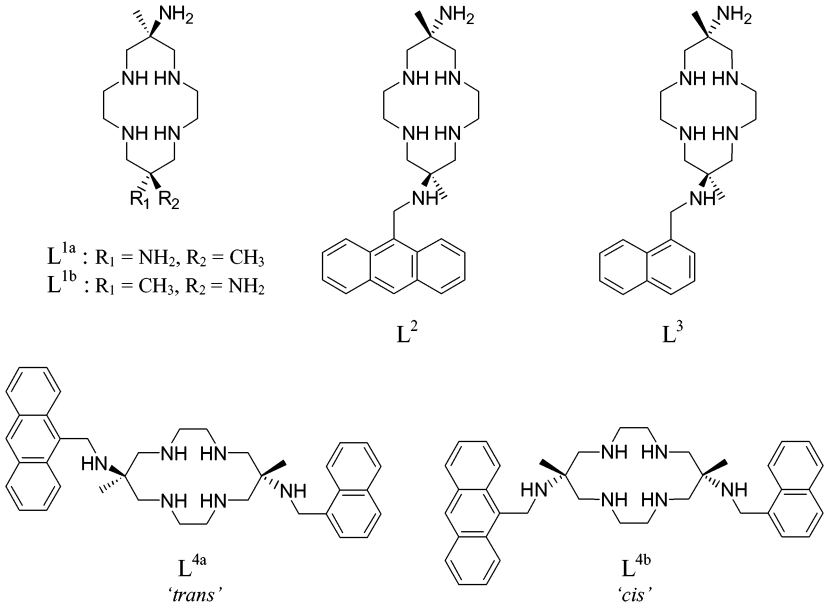

The Förster expression was originally formulated for long-range intermolecular energy transfer in bimolecular systems. Since this early work, significant progress in understanding the phenomenon of EET has been accomplished, from both theoretical and experimental viewpoints.[11,12] In cases where EET proceeds via an allowed singlet−singlet transition, such as that expected between two aromatic chromophores,[12] both the Coulombic and exchange interactions should be considered since, in both cases, the values of J_{dd} and J_{ex} may be nonvanishing.

The first observation of intramolecular EET between the naphthalene and anthracene aromatic chromophores was reported by Schnepp and Levy[13] where the linker was a simple alkyl chain of varying length. Subsequent investigations of these alkyl linked systems have been performed in solution,[14] as supersonic jet expansions[15] and in stretched polymer films[16] in order to elucidate the mechanisms responsible for the highly efficient (>99%) excitation energy transfer observed. More recently, Scholes et al.[17] reported on EET between the naphthalene and anthracene chromophores with a rigid bis(norbornyl)-bicyclo[2.2.0]hexane bridge which held the chromophores in a well-defined orientation and separation. The dominant pathway of EET was attributed to a through bond exchange interaction mediated by orbital overlap of the bridge with donor and acceptor orbitals.

Recently, we reported[18] highly efficient intramolecular EET between several aromatic chromophores appended to the parent L^{1a} macrocycle (Chart 1) when complexed to Zn(II). Herein, we report the rate constants of EET in the cis and trans isomers of L^1 asymmetrically disubstituted with naphthalene donor and anthracene acceptor chromophores as determined by time-resolved fluorescence studies. We show that this structural modification brings about a significant variation in the observed rate of EET, and the likely solution conformations of these dyads have been examined using molecular mechanics calculations.

Experimental Section

Synthesis. The parent macrocycles, *trans*- and *cis*-6,13-dimethyl-1,4,8,11-tetraaza-cyclotetradecane-6,13-diamine hexahydrochloride (L^{1a}·6HCl and L^{1b}·6HCl), were prepared according to previously reported methods.[19] Syntheses of the monosubstituted model compounds, L^2 and L^3, and the trans disubstituted bichromophore, L^{4a}, have similarly been previously reported.[18,20,21] L^{4b} was prepared with slight modifications to the procedure detailed elsewhere[18] using L^{1b} as the parent macrocycle, with full experimental details given as a supplement (see section S1 of the Supporting Information). Corresponding Zn(II) complexes of all ligands were generated in situ by titration with ∼1.1 equiv of $Zn(ClO_4)_2$·$6H_2O$. Unless otherwise stated, all other reagents were obtained commercially and used without further purification.

Physical Methods. Nuclear magnetic resonance spectra were measured at 400.13 (^{1}H) and 100.62 MHz (^{13}C) on a Bruker AV400 spectrometer using CD_3CN as the solvent and referenced to the residual solvent peak at 1.93 ppm. Electronic absorption spectra were measured on a Perkin-Elmer Lambda 40 spectrophotometer using quartz cells. Steady-state emission and excitation spectra were collected on a Perkin-Elmer LS-50B spectrofluorimeter. Samples were purged with N_2 prior to measurements and cut off filters were employed to avoid detection of higher order excitation light. Time-resolved fluorescence measurements were performed by time-correlated single photon counting (TCSPC). The light source was a Kerr lens modelocked Ti:sapphire laser (Tsunami, Spectra-Physics) pumped by a Nd:YVO_4 laser (Millenia, Spectra-Physics). Output pulses at a repetition rate of 82 MHz and a duration of 80−100 fs were tuned between 780 and 825 nm. About 260 mW of this output was frequency doubled in a 0.5 mm type I BBO crystal. These pulses were used for direct excitation of the anthracene chromophore. For excitation of the naphthalene energy donor, pulses at 275 nm were generated by sum frequency generation with the fundamental infrared and the frequency-doubled pulses in a 0.2 mm type I BBO crystal. The fluorescence was collected at 90° and filtered through appropriate band-pass filters. A polarizer orientated at a magic angle relative to the polarization of the excitation pulses was placed in front of the photomultiplier tube (Hamamatsu, H5783-P-01), with the detector output connected to the input of a TCSPC computer board module (Becker and Hickl, SPC-300-12). The full width at half-maximum of the instrument response function was less than 150 ps. Fluorescence time profiles were analyzed by iterative recon-

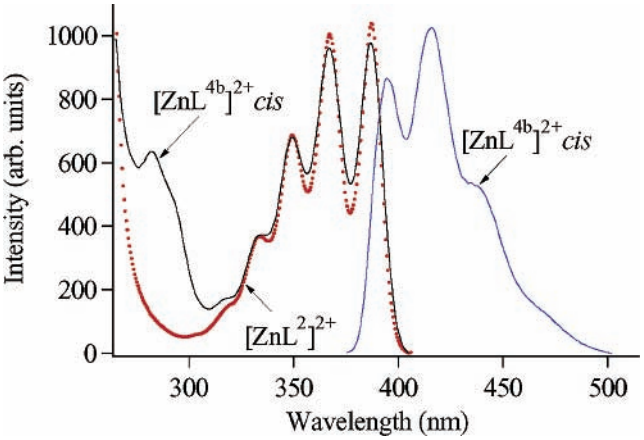

Figure 1. Fluorescence excitation spectra ($\lambda_{em} = 413$ nm) of $[ZnL^2]^{2+}$ (●) and $[ZnL^{4b}]^{2+}$ complexes (—) in CH_3CN solvent at 298 K. Also shown is the characteristic anthracene emission of $[ZnL^{4b}]^{2+}$ after naphthalene excitation ($\lambda_{ex} = 275$ nm).

volution with the response function using a nonlinear least-squares fitting procedure (MATLAB, The MathWorks Inc.).

Molecular Modeling. Molecular modeling of the Zn(II) complexes of L^{4a} and L^{4b} was performed with MOMEC97[22] using previously reported force field parameters[23] in order to evaluate the most likely conformations of these two molecules in solution. A tetragonally elongated octahedral coordination environment about the metal ion was assumed in both cases by comparison to the reported structure[18] of a disubstituted bis-(naphthalen-1-yl-methyl)amino derivative of L^{1a}. The complexes were modeled with four nitrogen donor atoms provided by tetradentate coordination of the macrocycle in the common *trans*-III and *trans*-I isomeric forms[24] to give an equatorial N_4 plane with two solvent CH_3CN molecules bound in axial positions completing the first coordination sphere.

Results

Steady-State Measurements. Absorption, excitation, and emission spectra for the Zn(II) complex of L^{4a}, the trans asymmetrically disubstituted macrocycle, have been previously reported[18] with MeOH as the solvent and analogous spectra for the Zn(II) complex of the cis isomer, L^{4b}, were found to be essentially identical. In both cases, absorption spectra were effectively a superposition of the spectra of the naphthalene and anthracene chromophores. The two most intense maxima at 223 and 254 nm have been attributed to the naphthalene and anthracene $S_0 \rightarrow S_3$ transitions, respectively.[18] At slightly lower energy, the naphthalene $S_0 \rightarrow S_2$ transition and anthracene $S_0 \rightarrow S_1$ transitions were evident, the former as a shoulder at ca. 275 nm and the latter as a well-defined Franck−Condon vibrational progression with an origin at 385 nm and several peaks to higher energy separated by ca. 1420 cm^{-1}.

Fluorescence excitation and emission spectra of the $[ZnL^{4b}]^{2+}$ cis complex and the excitation spectra of the related monosubstituted compound, $[ZnL^2]^{2+}$ in CH_3CN are shown in Figure 1. The corresponding spectra of the $[ZnL^{4a}]^{2+}$ trans complex are essentially identical, both in this solvent and as previously reported in MeOH.[18] A comparison of the fluorescence excitation spectra for $[ZnL^2]^{2+}$ and the bichromophoric $[ZnL^{4b}]^{2+}$ cis complex, monitoring the anthracene emission at 413 nm clearly shows new peaks in the latter. The fluorescence excitation spectra of the $[ZnL^{4a}]^{2+}$ trans complex (data not shown) was again essentially identical to that of the $[ZnL^{4b}]^{2+}$ cis complex. These new features correspond to absorption by the naphthalene chromophore resulting in emission that is characteristic of

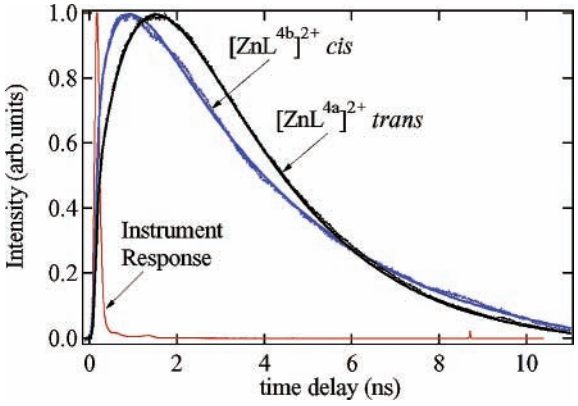

Figure 2. Instrument response function and fluorescence decay profiles for $[ZnL^{4a}]^{2+}$ trans and $[ZnL^{4b}]^{2+}$ cis in CH_3CN at 298K showing rise and decay of anthracene centered fluorescence ($\lambda_{em} > 400$ nm) following naphthalene centered excitation ($\lambda_{ex} = 275$ nm). Experimental data (points) were fitted (solid line) to an exponential rise and decay function (see text).

TABLE 1: Experimentally Determined Anthracene Radiative Lifetimes (τ) Measured Directly ($\lambda_{ex} = 390$ nm) and Indirectly ($\lambda_{ex} = 275$ nm) Together with the Observed Energy Transfer Rate Constants (k_{EET})

complex	$\tau_{(direct)}$ (ns)	$\tau_{(indirect)}$ (ns)	$k_{EET(exp)}$ (s^{-1})
$[ZnL^{4a}]^{2+}$ *trans*	2.61 ± 0.13	2.55 ± 0.13	$8.70 \pm 0.43 \times 10^8$
$[ZnL^{4b}]^{2+}$ *cis*	3.84 ± 0.19	3.90 ± 0.19	$2.33 \pm 0.12 \times 10^9$

anthracene. Excitation of the naphthalene chromophore in both the $[ZnL^{4a}]^{2+}$ trans and $[ZnL^{4b}]^{2+}$ cis complexes ($\lambda_{ex} = 275$ nm) yield emission spectra identical to those obtained upon direct excitation of the anthracene moiety at 390 nm, providing clear evidence of highly efficient electronic energy transfer (EET) operating in both these complexes.

Time-Resolved Measurements. Fluorescence lifetimes of the anthracene chromophore in the Zn(II) complexes of L^{4a} and L^{4b} were found to be 2.61 ± 0.13 and 3.84 ± 0.19 ns, respectively, when measured by direct excitation of the anthracene $S_0 \rightarrow S_1$ transition ($\lambda_{ex} = 390$ nm). At this wavelength, absorption by the naphthalene chromophore is negligible. The fluorescence decay curves shown in Figure 2 were collected with 275 nm excitation corresponding to excitation into the naphthalene $S_0 \rightarrow S_2$ transition and monitoring emission solely from the anthracene chromophore at $\lambda_{em} > 400$ nm. These curves were fit to a biexponential rise and decay function of the form shown in eq 6

$$I(t) = A_0 + A_1\left(\left(\frac{k_{EET}}{k_{EET} - k_1}\right)\exp^{(-k_1 t)} - \left(\frac{k_{EET}}{k_{EET} - k_1}\right)\exp^{(-k_{EET} t)}\right) \quad (6)$$

where $I(t)$ is the fluorescence intensity at time t, A_0 is a vertical offset, A_1 is a preexponential scaling factor, k_{EET} is the rate constant for energy transfer between chromophores, and k_1 is the radiative decay rate constant of the anthracene excited state (see section S2 of the Supporting Information).

From the fitting of eq 6 to the experimental data, the experimental rate constants of EET in the $[ZnL^{4a}]^{2+}$ trans and $[ZnL^{4b}]^{2+}$ cis complexes were determined to be $k_{EET} = 8.70$ (± 0.43) $\times 10^8$ and 2.33 (± 0.12) $\times 10^9$ s^{-1}, respectively, with corresponding fluorescence lifetimes ($\tau = 1/k_1$) for the anthracene chromophore of 2.55 ± 0.13 and 3.90 ± 0.19 ns. These results are summarized in Table 1 and compare well both with the values measured directly and the reported value ($\tau = 3.95$ ns) for 9-methylanthracene in hexane at 25 °C.[25] Notably, the

CHART 2: Various N-Based Isomeric Forms of the $[Zn(L^{4a})(CH_3CN)_2]^{2+}$ trans Complex that Were Modeled (See Text) with Axial CH_3CN Molecules Omitted for Clarity

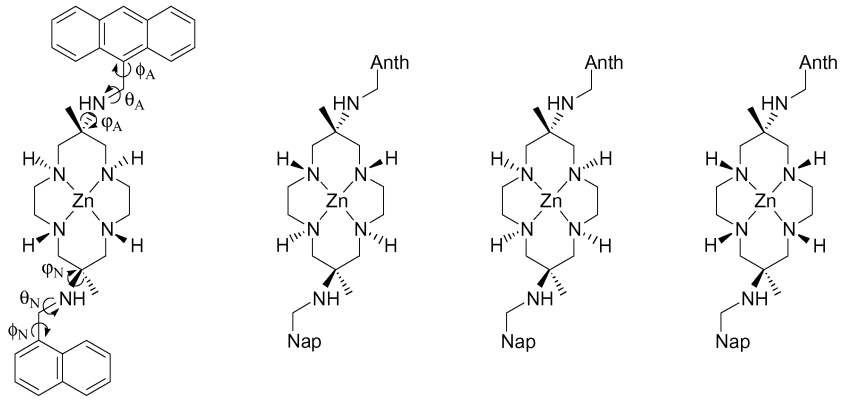

(i) $\alpha_A\alpha_N$-*trans*-III (ii) $\beta_A\beta_N$-*trans*-III (iii) $\alpha_A\beta_N$-*trans*-I (iv) $\beta_A\alpha_N$-*trans*-I

CHART 3: Various N-Based Isomeric Forms of the $[Zn(L^{4b})(CH_3CN)_2]^{2+}$ cis Complex that Were Modeled (See Text) with Axial CH_3CN Molecules Omitted

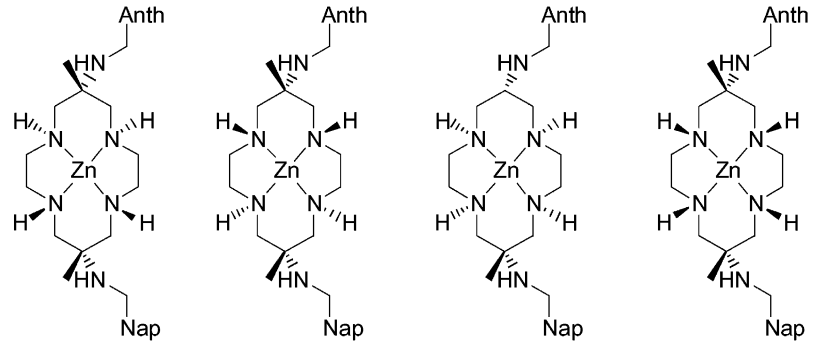

(i) $\alpha_A\beta_N$-*trans*-III (ii) $\beta_A\alpha_N$-*trans*-III (iii) $\alpha_A\alpha_N$-*trans*-I (iv) $\beta_A\beta_N$-*trans*-I

radiative lifetime of the anthracene chromophore in the $[ZnL^{4a}]^{2+}$ trans compound is significantly shorter than in the corresponding $[ZnL^{4b}]^{2+}$ cis isomer. A possible rationale for this observation is heavy-atom induced enhancement of inter-system crossing in the former case, due to a more proximal Zn(II) ion. The quantum efficiency of the EET reaction, Q, was estimated using the experimentally determined rate constants, k_{EET}, and the fluorescence lifetime ($\tau_D = 93.8$ ns) of 1-methyl-naphthalene[27] as the model donor chromophore according to eq 7

$$Q = k_{EET}/(k_{EET} + 1/\tau_D) \qquad (7)$$

Hence, the EET efficiencies for the $[ZnL^{4a}]^{2+}$ trans and $[ZnL^{4b}]^{2+}$ cis complexes were 98.8% and 99.5% respectively.

Molecular Modeling. Zn(II) complexes of L^{4a} coordinated in the *trans*-III isomeric form can exist as two configurational diastereomers, namely, the α-*trans*-III or β-*trans*-III forms,[26] whereby the pendant nitrogen atom is on the same or opposite side of the macrocyclic N_4 plane as the adjacent coordinated secondary amine protons, respectively. As a result of this N-based isomerism, the pendant naphthalene and anthracene chromophores will both adopt either axial (e.g., $\alpha_A\alpha_N$) or equatorial (e.g., $\beta_A\beta_N$) dispositions (see Chart 2i,ii) with respect to their attached six membered chelate rings, resulting in conformations that differ significantly both in orientation and separation of the chromophores. Conversely, upon tetradentate coordination of L^{4a} in the *trans*-I mode, the trans pendant amines will result in the chromophores adopting opposing dispositions (e.g., $\alpha_A\beta_N$ or $\beta_A\alpha_N$) as shown in Chart 2iii,iv. For L^{4b}, the situation is reversed due to the cis disposition of the pendant amine nitrogens in that coordination in the *trans*-III mode will orient the chromophores dissimilarly (e.g., $\alpha_A\beta_N$, $\beta_A\alpha_N$; see Chart 3i,ii), whereas coordination in the *trans*-I mode will give $\alpha_A\alpha_N$ or $\beta_A\beta_N$ orientations as depicted in Chart 3iii,iv. It has been shown that the rate of N-based isomerization in the Cu(II) complexes of the parent macrocycles (L^{1a} and L^{1b}) is negligible, with no interconversion between these forms after metal ion complexation.[26] A similar situation will hold for the Zn(II) complexes of L^{4a} and L^{4b} which necessitated modeling the differing N-based isomeric forms as separate, noninterconvertible conformational ensembles.

Hence, for $[Zn(L^{4a})(CH_3CN)_2]^{2+}$ in the $\alpha_A\alpha_N$-*trans*-III form shown in Chart 2i, and considering the torsional angles labeled θ_A, ϕ_A, and φ_A as shown, conformational analysis of the ideal gauche orientations (with $\theta_A = \pm 60°$, 180°; $\phi_A = \pm 30°$, $\pm 90°$, $\pm 150°$; and $\varphi_A = \pm 60°$, 180°) results in a total of 54 possible combinations. Of these, a total of 46 conformers including all those with $\varphi_A = 180°$ were rejected because of severe steric clashing. In addition, only the N-based isomers that conserve the H-bonding interaction between the pendant amine lone pair and the adjacent coordinated secondary amine protons were considered. This resulted in eight 2-fold degenerate conformational starting points which were further refined to yield eight strain energy minima at the anthracene appended end of the macrocycle. Notably, the lowest energy minimum of these ($\theta_A = +57.7°$, $\phi_A = 61.1°$, and $\varphi_A = \pm 53.2°$) closely resembles the solid state structure previously reported[20] for $[Cu(L^2)(ClO_4)_2]$. A similar treatment for θ_N, ϕ_N, and φ_N yielded 20 strain energy minima for the naphthalene appended fragment, again with the lowest energy minimum closely resembling the

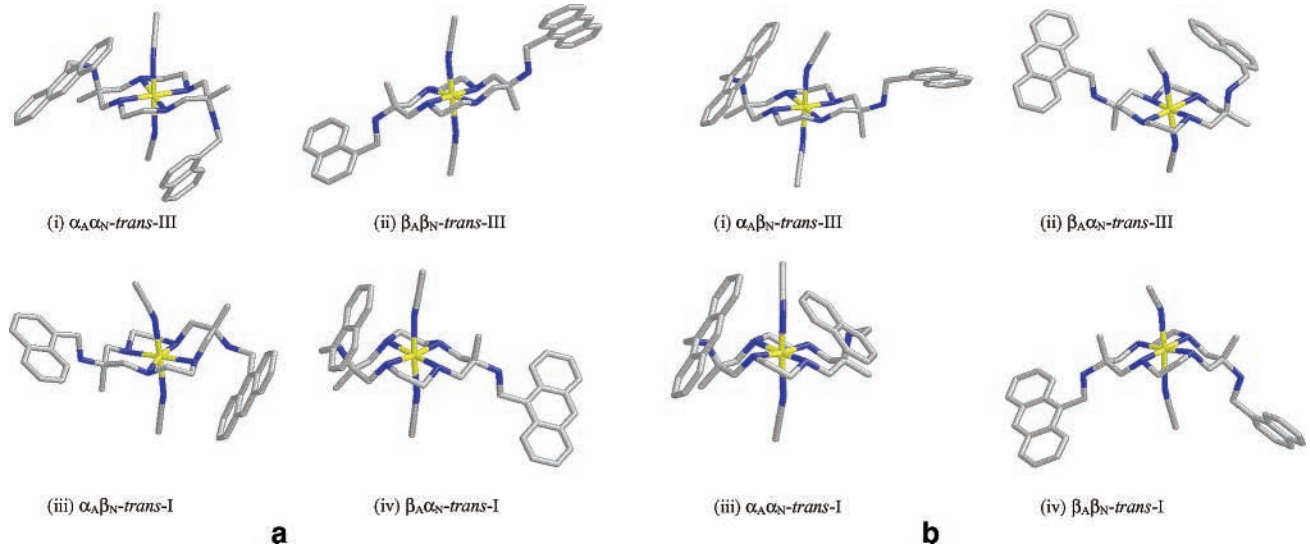

Figure 3. (a) Lowest strain energy minimized structures for the various *trans*-III and *trans*-I N-based isomeric forms of the $[Zn(L^{4a})(CH_3CN)_2]^{2+}$ trans complex that were modeled. (b) Lowest strain energy minimized structures for the various *trans*-III and *trans*-I N-based isomeric forms of the $[Zn(L^{4b})(CH_3CN)_2]^{2+}$ cis complex that were modeled.

orientation observed crystallographically[21] for $[Cu(L^3)(ClO_4)_2]$. The combination of these lowest energy conformations for each end of the macrocycle yielded a total of 160 (20 × 8) conformations which were modeled for L^{4a} coordinated to Zn(II) in the $\alpha_A\alpha_N$-*trans*-III form. In the $\beta_A\beta_N$-*trans*-III form (Chart 2ii), with both pendant groups oriented equatorially, the situation is somewhat more complex with increased flexibility of the appended groups because of the more sterically accommodating equatorial disposition of the chromophores. Again, treating each end independently, conformational analysis revealed a total of 10 possible conformations for the anthracene appended end of the macrocycle and 27 at the naphthalene end of the macrocycle which combine to give a total of 270 (27 × 10) conformations which were modeled. For the $[Zn(L^{4a})(CH_3CN)_2]^{2+}$ complex, with macrocyclic coordination in the *trans*-I mode, there exist 216 (8 × 27) and 200 (10 × 20) minima for the $\alpha_A\beta_N$ and $\beta_A\alpha_N$ forms, respectively, which were modeled. For each of these N-based isomeric forms of the $[Zn(L^{4a})(CH_3CN)_2]^{2+}$ trans complex, the resulting lowest energy strain minimized structures are shown in Figure 3a.

Upon tetradentate coordination of L^{4b} to Zn(II) in the *trans*-III isomeric form, for the $\alpha_A\beta_N$-*trans*-III orientation depicted in Chart 3i, there are again only 8 strain energy minima which need be considered for the axially oriented anthracene fragment and 27 conformations for the equatorially disposed naphthalene fragment resulting in a total of 216 (8 × 27) conformations which were modeled. For $[ZnL^{4b}]^{2+}$ in the $\beta_A\alpha_N$-*trans*-III orientation depicted in Chart 3ii, the axially disposed naphthalene may again adopt 20 differing conformations, whereas the C_{2v} symmetry of the equatorial anthracene fragment results in only 10 strain energy minima which, in combination, give a total of 200 (20 × 10) conformations which were modeled. The *trans*-I coordination mode orients both chromophores either axially or equatorially. In the former case, there exist 160 (8 × 20) minima for the $\alpha_A\alpha_N$-*trans*-I mode (see Chart 3iii) that were modeled, whereas for the latter, 270 (10 × 27) conformations were modeled for the $\beta_A\beta_N$-*trans*-I isomer (see Chart 3iv). Again, for each of these N-based isomeric forms of the $[Zn(L^{4b})(CH_3CN)_2]^{2+}$ cis complex, the resulting lowest energy strain minimized structures are shown in Figure 3b.

Rate Calculations. The contribution to the overall rate constant of energy transfer via a Coulombic (dipole−dipole) mechanism can be evaluated using the Förster expression (eq 2). The refractive index, n, of CH_3CN was taken to be 1.344. Literature values of 93.8 ns and 0.40 for the fluorescence lifetime, τ_D, and fluorescence quantum yield, Φ_D, of 1-methylnaphthalene as the model donor chromophore were used.[27,28] The spectral overlap integral J_{dd} was determined experimentally to be $\sim 1.2 \times 10^{-15}$ mol^{-1} cm^6 using the previously reported[21] normalized emission spectrum of $[ZnL^3]^{2+}$ and the absorption spectrum of $[ZnL^2]^{2+}$. The interchromophore separation, R, between the center of the naphthalene and anthracene chromophores (see Figure 4) was evaluated with the aid of the modeled structures for each strain energy minimized conformation. Lastly, the orientation factor was similarly determined using the modeled structures. Given the lowest energy excited singlet states of the naphthalene and anthracene chromophores are ^1L_b (long axis polarized) and ^1L_a (short axis polarized), respectively, and EET is normally assumed to occur between these states,[17] the orientation factor, κ, for each strain energy minimized structure was determined using eq 8

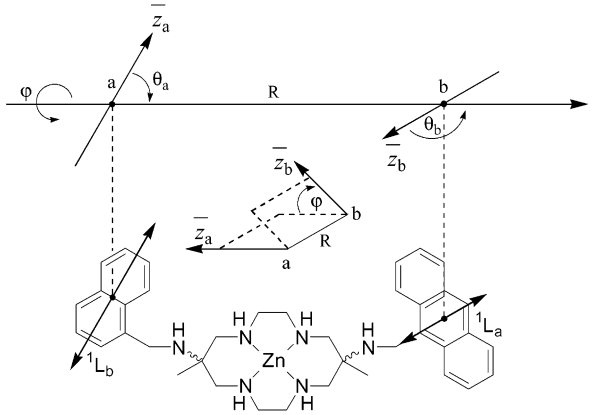

Figure 4. Dipole moment vectors for naphthalene, $\bar{z}_a$ (^1L_b transition, long axis polarized) and anthracene, $\bar{z}_b$ (^1L_a transition, short axis polarized) and hence the angles θ_a, θ_b and φ used to determine the orientation factor, κ^2. Points "a" and "b" were taken as the center of the naphthalene and anthracene aromatic ring systems, respectively.

$$\kappa = (2 \cos\theta_a \cos\theta_b - \sin\theta_a \sin\theta_b \cos\varphi) \qquad (8)$$

where θ_a and θ_b are the angles subtended by the dipole moment

TABLE 2: Summary of Results from Molecular Modeling Studies for the Lowest Strain Energy Conformers Shown in Figure 3 for Each N-Based Isomeric Form[a]

complex	N-based isomer	strain energy minima (kJ mol^{-1})	R (Å)	κ^2	k_{EET} (calc'd) (s^{-1})	k_{EET} (calc'd) (all conformers) (s^{-1})
$[Zn(L^{4a})(CH_3CN)_2]^{2+}$ trans	$\alpha_A\alpha_N$-*trans*-III	105.13	8.78	0.71	2.13×10^9	1.09×10^9
	$\beta_A\beta_N$-*trans*-III	120.46	16.44	0.01	5.41×10^5	2.33×10^7
	$\alpha_A\beta_N$-*trans*-I	122.29	12.45	1.03	3.82×10^8	2.48×10^8
	$\beta_A\alpha_N$-*trans*-I	124.38	12.95	0.03	7.37×10^6	2.27×10^8
$[Zn(L^{4b})(CH_3CN)_2]^{2+}$ cis	$\alpha_A\beta_N$-*trans*-III	110.36	11.82	1.19	6.02×10^8	0.38×10^9
	$\beta_A\alpha_N$-*trans*-III	113.45	11.05	2.53	1.92×10^9	1.08×10^9
	$\alpha_A\alpha_N$-*trans*-I	112.65	7.04	0.55	6.16×10^9	3.22×10^9
	$\beta_A\beta_N$-*trans*-I	132.14	13.75	0.46	9.28×10^7	2.38×10^8

[a] The calculated overall Boltzmann weighted energy transfer rate for all conformers in each N-based isomeric ensemble are also shown in the last column.

vector of donor and acceptor chromophores respectively on the interchromophore separation vector $\vec{ab}$ as shown in Figure 4 and φ is the torsional angle about this vector. The results of these calculations are given for the strain energy minima conformation of each N-based isomeric form (see Figure 3a,b) in Table 2.

To determine the overall calculated rate constant, it was assumed the distribution of conformers within each N-based isomeric form shown in Charts 2 and 3 followed a Boltzmann distribution and that the rate of energy transfer was much faster than interconversion between conformers. The probability $p(i)$ of finding a conformer i within a particular N-based ensemble is then given by eq 9[29]

$$p(i) = \exp\left(\frac{-E_i}{kT}\right) / \sum_j \exp\left(\frac{-E_j}{kT}\right) \qquad (9)$$

where E_i is the minimized strain energy of the i conformer, k is the Boltzmann constant, and T was the temperature (298 K). The resulting probability distributions for each N-based isomeric ensemble as a function of R, the interchromophore separation, are shown in Figure 5, parts a and b for the trans and cis complexes, respectively. These were then used to calculate the relative contribution of each conformer to the overall rate of EET, the results of which are summarized in Table 2.

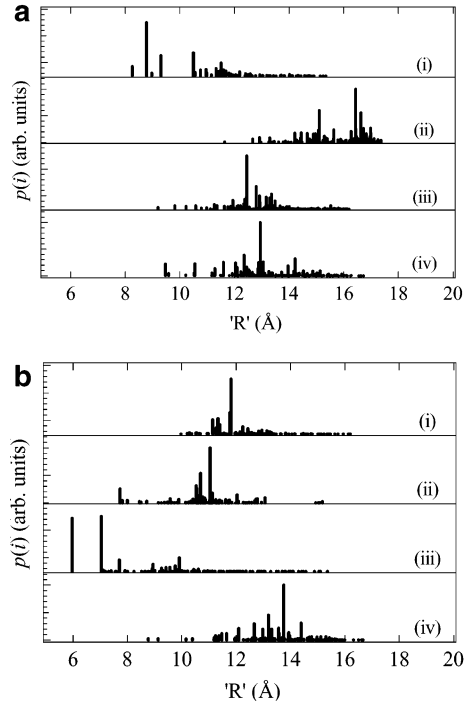

Figure 5. (a) Conformational probability distributions for the various N-based isomeric forms of the $[Zn(L^{4a})(CH_3CN)_2]^{2+}$ trans complex that were modeled (see Chart 2) (i) $\alpha_A\alpha_N$-*trans*-III, (ii) $\beta_A\beta_N$-*trans*-III, (iii) $\alpha_A\beta_N$-*trans*-I, and (iv) $\beta_A\alpha_N$-*trans*-I. (b) Conformational probability distributions for the various N-based isomeric forms of the $[Zn(L^{4b})(CH_3CN)_2]^{2+}$ cis complex that were modeled (see Chart 3) (i) $\alpha_A\beta_N$-*trans*-III, (ii) $\beta_A\alpha_N$-*trans*-III, (iii) $\alpha_A\alpha_N$-*trans*-I, and (iv) $\beta_A\beta_N$-*trans*-I.

Discussion

The results from steady-state measurements for the Zn(II) complexes of the isomeric trans L^{4a} and cis L^{4b} ligands in CH_3CN clearly demonstrate the presence of an intramolecular energy transfer pathway which efficiently quenches naphthalene fluorescence. With the experimentally determined rate constants of EET, the quantum efficiency of EET was estimated to be approximately 99% in both cases, which is comparable to the flexible alkyl chain linked bichromophores first reported by Schnepp and Levy[13] and the more recent rigidly linked polynorbornyl bichromophores of Scholes et al.[17] To account for the highly efficient energy transfer in the $[ZnL^{4a}]^{2+}$ trans and $[ZnL^{4a}]^{2+}$ cis complexes, several EET mechanisms were considered.

The contributions to the overall rate of energy transfer from a direct exchange (Dexter type) mechanism were neglected since the large interchromophore separations in this case greatly exceed that required for direct through space orbital overlap of donor and acceptor chromophores. The possibility of a through-bond (TB) coupled exchange interaction, whereby orbital overlap is mediated by the connecting bridge, was considered. Although more common for linkers comprising extended π systems, the utilization of σ bond spacers to promote efficient long-range EET via a TB superexchange pathway has been demonstrated by Closs et al.[30] for triplet−triplet based EET and more recently for singlet−singlet EET by Scholes et al.[17] In both these cases, however, the interaction was observed between rigidly linked bichromophoric molecules. For the Zn(II) complexes of both L^{4a} and L^{4b} considered here, although the macrocycle itself could be considered as a rigid bridge, the inherent flexibility of the appended chromophores, as demonstrated by molecular modeling, would act to minimize these TB interactions.

Energy transfer rate constants obtained via a direct Coulombic (Förster type) interaction between the two chromophores were estimated from the modeled structures. For the $[Zn(L^{4a})(CH_3CN)_2]^{2+}$ trans complex, it was found that the four *trans*-III and *trans*-I N-based isomeric forms which were modeled gave markedly different calculated rate constants for excitation transfer (Table 2). The origin of these differences is clearly shown in Figure 5a, which reveals largely dissimilar interchro-

mophore separations for these N-based isomeric forms of the $[Zn(L^{4a})(CH_3CN)_2]^{2+}$ trans complex. The dominant conformer of the $\alpha_A\alpha_N$-*trans*-III form, as shown in Figure 3a, has axially oriented chromophores which are neatly folded on either side of the macrocycle allowing a close approach of the naphthalene and anthracene moieties. By contrast, the dominant conformer of the $\beta_A\beta_N$-*trans*-III form (Figure 3a), with equatorially disposed chromophores, adopts a much more extended conformation with a corresponding increase in the interchromophore separation and hence the rate of EET. The two *trans*-I N-based isomeric forms both have similar rate constants of excitation transfer, which is intermediate between those calculated for the $\alpha_A\alpha_N$-*trans*-III and $\beta_A\beta_N$-*trans*-III forms. This can be rationalized by inspection of Table 2, which reveals the dominant conformers within these *trans*-I isomeric forms have an intermediate interchromophore separation.

The time-resolved fluorescence experiments for $[ZnL^{4a}]^{2+}$ were determined for complexes generated in situ by titration with a 5% excess of $Zn(ClO_4)_2 \cdot 6H_2O$. First, given the many possible isomeric forms of each complex, NMR spectroscopy of the resulting solutions was examined. Each noninterconvertable N-based isomeric form will result in one pair of methyl (singlet) resonances (of equal intensity) in the ^{1}H NMR spectrum, due to the different shielding effects of the adjacent naphthyl and anthryl groups. The ^{1}H NMR spectrum of $[ZnL^{4a}]^{2+}$ clearly shows the appearance of two pairs of methyl resonances in an approximate 3:1 ratio indicating the presence of only two major N-based isomers in solution (see Figure S3-(a) of the Supporting Information). Using the strain energies of the modeled compounds as a guide, it seems likely that the major isomer in solution would correspond to the $\alpha_A\alpha_N$-*trans*-III isomer. In addition, the presence of two bifurcated H-bonding interactions at either end of the macrocycle between protons of the coordinated secondary amines and the pendant nitrogen stabilize this conformer and may account for its preferential formation in solution. Indeed, it is typically this isomeric form that is observed crystallographically for all substituted derivatives of L^{1a} examined to date. The identity of the minor isomer remains uncertain given the similarity of the minimized strain energies. However, it is notable that the differences in chemical shift for the methyl peaks between the two isomers are not the same, with a larger change apparent for the methyl peak adjacent to the appended naphthalene fragment. This larger change may correspond to the difference between an axially versus equatorially oriented naphthalene fragment which would indicate the other species present in solution is likely the $\alpha_A\beta_N$-*trans*-I isomer.

The markedly different rate constants calculated for these two modeled isomeric forms of the $[Zn(L^{4a})(CH_3CN)_2]^{2+}$ trans complex would be expected to give a biexponential rise in anthracene fluorescence. However, the estimated rise time ($1/k_{EET}$) of ~4 ns for the $\alpha_A\beta_N$-*trans*-I form (or indeed the $\beta_A\alpha_N$-*trans*-I (4.4 ns) and $\beta_A\beta_N$-*trans*-III (42.9 ns) forms) combined with the comparatively rapid deactivation of the anthracene acceptor ($\tau = 2.61$ ns) results in the slower conformer being concealed within the 12.2 ns time frame of the TCSPC experiment. Hence, the experimental data was satisfactorily fit to a single-exponential rise with the rate constant of $k_{EET} = 8.7 \times 10^8$ s^{-1} in excellent agreement with that predicted by molecular modeling for the dominant $\alpha_A\alpha_N$-*trans*-III form of the complex.

For the cis isomer, $[ZnL^{4b}]^{2+}$, the experimentally determined rate constant for EET was found to be 2.33×10^9 s^{-1} which is intermediate between those predicted by the direct Coulombic mechanism for the *trans*-III and *trans*-I N-based isomeric forms (see Table 2). As was the case for L^{4a}, time-resolved measurements for the $[ZnL^{4b}]^{2+}$ system were conducted with Zn(II) complexation performed in situ. The ^{1}H NMR spectrum of this complexation reaction with L^{4b} is far more complicated than the corresponding spectra for L^{4a}, showing the appearance of several pairs of methyl resonances (see Figure S3(b) of the Supporting Information) indicating there are several N-based isomeric forms of the $[ZnL^{4b}]^{2+}$ complex present in solution. Unfortunately, because of the degeneracy of several methyl peaks, the ^{1}H NMR spectrum cannot be unambiguously assigned and the relative proportions of these N-based isomers cannot be accurately determined. Notably, however, as was mentioned in the case of the $[ZnL^{4a}]^{2+}$ system, the presence of two bifurcated H-bonding interactions between the protons of coordinated secondary amines and the pendant nitrogen is again evident only in the $\alpha_A\alpha_N$-*trans*-I isomeric form of the $[Zn(L^{4b})]^{2+}$ complex, and this may be the dominant N-based isomer in solution. Regardless, the close agreement obtained with the experimental results is indicative of a predominantly Förster type mechanism responsible for the observed EET in both the $[ZnL^{4a}]^{2+}$ and $[ZnL^{4b}]^{2+}$ complexes.

Time-resolved investigations of the energy transfer rates for each N-based isomeric form in isolation would undoubtedly simplify the analysis. However, chromatographic separation and isolation of the various N-based isomeric forms of both $[ZnL^{4a}]^{2+}$ and $[ZnL^{4b}]^{2+}$ complexes has not been possible.

Conclusions

The rate constant of EET in the Zn(II) complex of the trans isomer of an asymmetrically disubstituted macrocyclic bichromophore, $[ZnL^{4a}]^{2+}$, follows a simple Coulombic interaction between the naphthalene and anthracene chromophores. As evident from the molecular modeling study, this complex can exist in a wide variety of conformations within the dominant $\alpha_A\alpha_N$-trans-III N-based isomeric form through simple C−C or C−N bond rotation about the exocyclic amino groups. Similarly, the possibility of differing N-based isomers within the macrocyclic core lead to minimal relayed Coulombic and through-bond exchange type interactions as is the case with other flexibly linked systems.

For the corresponding cis isomer, $[ZnL^{4b}]^{2+}$, the rate of EET can similarly be understood with a simple Coulombic interaction between chromophores. The faster rate constant observed experimentally can be attributed to a greater variety of isomeric forms being available to this ligand when complexed with Zn(II), with a preference for the $\alpha_A\alpha_N$-*trans*-I isomeric form allowing a closer approach of the chromophores than for the corresponding $\alpha_A\alpha_N$-*trans*-III-$[Zn(L^{4a})]^{2+}$ *trans* complex.

Acknowledgment. E.G.M. gratefully acknowledges the award of a Graduate School Research Travel Award (GSRTA) from the University of Queensland and the Arlo D. Harris Travel Award from the Department of Chemistry.

Supporting Information Available: Full synthesis of L^{4b}, derivation of eq 6, and ^{1}H NMR spectra of $[ZnL^{4a}]^{2+}$ trans and $[ZnL^{4b}]^{2+}$ cis complexes. This material is available free of charge via the Internet at http://pubs.acs.org.

References and Notes

(1) Adronov, A.; Frechet, J. M. J. *Chem. Commun.* **2000**, *18*, 1701.
(2) Miller, M. A.; Lammi, R. K.; Prathapan, S.; Holten, D.; Lindsey, J. S. *J. Org. Chem.* **2000**, *65*, 6634.
(3) Harriman, A. *Photochemistry* **1998**, *29*, 425.

(4) Gust, D.; Moore, T. A. *Photosynth. React. Cent.* **1993**, *2*, 419.
(5) Raju, B. B.; Varadarajan, T. S. *J. Lumin.* **1993**, *55*, 49.
(6) Weller, H.; Grellmann, K. H. *J. Am. Chem. Soc.* **1983**, *105*, 6268.
(7) Adronov, A.; Robello, D. R.; Frechet, J. M. J. *J. Polym. Sci., Part A: Polym. Chem.* **2001**, *39*, 1366.
(8) Pei, J.; Liu, X.-L.; Yu, W.-L.; Lai, Y.-H.; Niu, Y.-H.; Cao, Y. *Macromolecules* **2002**, *35*, 7274.
(9) Förster, T. *Discuss. Faraday Soc.* **1959**, *27*, 7.
(10) Dexter, D. L. *J. Chem. Phys.* **1953**, *21*, 836.
(11) Scholes, G. D.; Ghiggino, K. P. *J. Chem. Phys.* **1994**, *101*, 1251.
(12) Speiser, S. *Chem. Rev.* **1996**, *96*, 1953.
(13) Schnepp, O.; Levy, M. *J. Am. Chem. Soc.* **1962**, *84*, 172.
(14) Nishimura, Y.; Yasuda, A.; Speiser, S.; Yamazaki, I. *Chem. Phys. Lett.* **2000**, *323*, 117.
(15) Wang, X.; Levy, D. H.; Rubin, M. B.; Speiser, S. *J. Phys. Chem. A* **2000**, *104*, 6558.
(16) Hasegawa, M.; Enomoto, S.; Hoshi, T.; Igarashi, K.; Yamazaki, T.; Nishimura, Y.; Speiser, S.; Yamazaki, I., *J. Phys. Chem. B* **2002**, *106*, 4925.
(17) Scholes, G.; Ghiggino, K.; Oliver, A.; Paddon-Row, N. *J. Phys. Chem.* **1993**, *97*, 11871.
(18) Bernhardt, P. V.; Moore, E. G.; Riley, M. J. *Inorg. Chem.* **2002**, *41*, 3025.
(19) Bernhardt, P. V.; Comba, P.; Hambley, T. W.; Lawrance, G. A.; Várnagy, K. *J. Chem. Soc., Dalton Trans.* **1992**, 355.
(20) Bernhardt, P. V.; Flanagan, B. M.; Riley, M. J. *J. Chem. Soc., Dalton Trans.* **1999**, *20*, 3579.
(21) Bernhardt, P. V.; Moore, E. G.; Riley, M. J. *Inorg. Chem.* **2001**, *40*, 5799.
(22) Comba, P.; Hambley, T. W. *Molecular Modeling of Inorganic Compounds*; VCH: Weinheim, Germany, 1995.
(23) Bernhardt, P. V.; Comba, P. *Inorg. Chem.* **1992**, *31*, 2638.
(24) Bosnich, B.; Poon, C. K.; Tobe, L. *Inorg. Chem.* **1965**, *4*, 1102.
(25) Blatt, E.; Treloar, E. F.; Ghiggino, K. P.; Gilbert, R. G. *J. Phys. Chem.* **1981**, *85*, 2810.
(26) Bernhardt, P. V.; Jones, L. A.; Sharpe, P. C. *J. Chem. Soc., Dalton Trans.* **1997**, 1169.
(27) Roek, D. P.; Chateaneuf, J. E.; Brennecke, J. F. *Ind. Eng. Chem. Res.* **2000**, *39*, 3090.
(28) Zvolinski, V. P.; Nizhegorodov, N. I. *Russ. J. Phys. Chem.* **1994**, *68*, 636.
(29) Schael, F.; Rubin, M. B.; Speiser, S. *J. Photochem. Photobiol. A, Chem.* **1998**, *115*, 99.
(30) Closs, G. L.; Piotrowiak, P.; MacInnis, J. M.; Fleming, G. R. *J. Am. Chem. Soc.* **1988**, *110*, 2652.